RSC Advances

ROYAL SOCIETY OF CHEMISTRY

www.rsc.org/advances

Biotemplated hierarchical porous-structure of ZnAl-LDH/$ZnCo_2O_4$ composites with enhanced adsorption and photocatalysis performance

Jing Yu, Lu Lu, Jia Li[1], Peng Song

School of Material Science and Engineering, University of Jinan, Jinan 250022, PR China

Abstract

Hierarchically porous ZnAl-LDH/$ZnCo_2O_4$ composites were synthesized by pine pollen via a two-step process involving self-assembly of $ZnCo_2O_4$ nanoparticles and hydrothermal synthesis of zinc aluminum layered double hydroxide with CO_3^{2-} as interlayer anion (abbreviated as ZnAl-LDH). The characteristics of the obtained samples were investigated by XRD, SEM, EDS, TEM, FTIR, BET and DRS. These results demonstrated that the synthesized ZnAl-LDH/$ZnCo_2O_4$ and its derived metal oxides all retained the structure of pine pollen grains. Layered ZnAl-LDH dispersed uniformly on the surface of the support of $ZnCo_2O_4$ ellipsoid. The adsorption of Congo red (CR) onto the as-synthesized samples was systematically investigated. The kinetic studies suggested that the adsorption process followed pseudo-second-order kinetic model. In addition, the catalytic activities of the obtained samples for CR degradation under simulative sunlight irradiation were also evaluated. It was found that the derived metal oxides exhibited better catalytic activity for CR degradation than ZnAl-LDH/$ZnCo_2O_4$ and the degrading efficiency of CR was about 91%.

Keywords: Biological template; Layered double hydroxides; Adsorption; Photocatalysis

1. Introduction

[1] Corresponding author: Tel: 8613953185430.
E-mail address: mse_lij@ujn.edu.cn

Nowadays, the problems of water pollution have become a global concern because of their impact on public health. Water contamination due to dyes from textiles, plastics, paper and coatings is a major environmental concern.[1-3] Therefore, it is very important to develop the technologies to prevent further dyes contamination. Semiconductor photocatalysis for degradation of organic pollutants in wastewater has become a topic of much interest owing to its simple decomposition process and effective use of solar energy.[4-6] Over the course of the past decades, TiO_2 has been widely studied due to its non-toxicity, low production cost, strong redox ability, high chemical stability, and superior efficiency in photocatalysis degradation.[7-10] While the wide band gap of 3.2 eV makes TiO_2 be utilized only within ultraviolet light range and leads to inefficient utilization of solar energy.[11-13] In order to make more efficient utilization of incident light energy, developing visible light responsive photocatalysts has become the most important topic in photocatalysis field .

Spinel compounds, as a novel semiconductor compounds, have become research hotspots because of their structure stability, photoelectrochemical stability and high repeatable utilization.[14-16] To date, a series of spinel oxides with high photocatalytic activity has been reported, such as $ZnFe_2O_4$,[17] Zn_2SnO_4,[18,19] $ZnCr_2O_4$,[20] $NiCo_2O_4$[21] and $BaCr_2O_4$.[22] Particularly, $ZnCo_2O_4$ not only has the unique properties of spinel structure, its excellent properties of electrochemical and gas sensitive also have been widely used in ceramics, gas sensors, supercapacitor and other fields.[23-25] Furthermore, $ZnCo_2O_4$ has been paid great attention because of its superior photocatalytic performance in visible light degradation of organic pollutants. $ZnCo_2O_4$ microspheres synthesized by Guo et al.[26] exhibited efficient photocatalytic activities in the degradation of methylene blue (MB) under visible-light illumination. $ZnCo_2O_4$ nanoparticles

prepared by Cui et al.[27] had been proved as an effective photocatalyst for decomposing MB into inorganic substances under visible light irradiation. Therefore, $ZnCo_2O_4$ appears to be a suitable choice which can be used in the degradation of organic pollutants in wastewater. Current catalysts mainly are nanomaterials, but nanostructure materials simultaneously cause many new problems, such as the troubles in separation and reutilization. The method of biological template can overcome these problems to some extent because of their larger size in microstructure.[28-30]

Due to the property of ease of preparation, biological templates have attracted more attention to fabricate porous structures.[31] Compared with inorganic templates, biological templates can provide a well-defined morphology in the preparation of micro and nano materials. Moreover, the catalyst which is synthesized by biological templates can possess hierarchically porous structure and higher surface area. And these can offer more active sites during the adsorption and catalysis process. In the past decades, there are a large amount of reports about the preparation of porous structures using biological agents as templates. He et al.[32] had successfully synthesized 3D hierarchical porous NiO by using ball-milled shells as biological template. Ma et al.[33] had obtained macro-mesoporous alumina using yeast cell as bio-template. ZrO_2 hollow porous microspheres was successfully prepared by Fan and her group using yeast as bio-templates.[34] On account of its unique ellipsoidal morphology, uniform particle size and higher surface area, pollen is an excellent candidate to be used as biological template. CeO_2 microspheres obtained by using lotus flower pollen as biological template exhibited high photocatalytic activity to remove MB under solar irradiation.[35] $FePMo_{12}/SiO_2$ synthesized by using camellia pollen as template had an enhanced photocatalytic activity to degrade the Acid Red 3R solution.[36] Considering the stability of catalytic performance, spinel $ZnCo_2O_4$ which is prepared by using pine pollen as the template has been

selected as the catalyst precursor in present work.

One of the attractive materials used to enhance photocatalytic activities of $ZnCo_2O_4$-based materials is layered double hydroxides (LDHs). LDHs, are generally expressed by the formula $[M_{1-a}^{2+}M_a^{3+}(OH)_2]^{a+}$ $(A^{b-})_{a/b}$ mH_2O (where M^{2+} is divalent metals; M^{3+} is trivalent metals like; A^{b-} is anions).[34-36] Moreover, calcined LDHs convert into well-dispersed mixed oxides with numerous porous structure and higher surface area.[40] On the basis of their special layer structure and versatility in chemical composition, LDHs and its derived metal oxides have been widely used in biology, adsorption and catalysis.[41-43] Due to their inherent positive charge and the rich ionic surface -OH group, LDH nanosheets can interact with other materials, generating 3-dimensional (3D) composites with specific architectures.[44] This feature inspires us to combine ZnAl-LDH nano-sheets and biomorphic $ZnCo_2O_4$ together for synthesizing the hierarchically porous composites, with the expectation to obtain pollen-like microspheres with open 3D hierarchically porous structure. And the calcined product of ZnAl-LDH can form a hybrid catalyst with $ZnCo_2O_4$ substrate. What other deserves to be mentioned is that because the porous $ZnCo_2O_4$ and flake-like LDHs both can be used as adsorbent, the hybrid catalyst also has good adsorption performance.

In this study, ZnAl-LDH/$ZnCo_2O_4$ composites and its derived metal oxides were synthesized via a biotemplated synthesis technique for the decomposition of Congo red (CR) in water. The adsorption performance and photocatalytic property of the catalyst were evaluated by the decolorization of CR aqueous solution. The purpose of this study is to develop a new approach to design and preparation of high performance materials in catalysis and adsorption.

2. Materials and methods

2.1 Materials

In this work, all reagents were used without further purification. Pine pollen was obtained from the local market. $Zn(NO_3)_2\ 6H_2O$ (AR Grade, Purity: P99.0%) and $Al(NO_3)_3\ 9H_2O$ (AR Grade, Purity: P98.0%) were purchased from Sinopharm Chemical Reagent Co., Ltd. $Co(NO_3)_3\ 6H_2O$ (AR Grade, Purity: P99.0%), urea (CON_2H_4, AR Grade, Purity: P99.0%) and Congo red ($C_{32}H_{22}N_6Na_2O_6S_2$, Dye content, P85.0%) were obtained from Tianjin Chemical Reagent Co., Ltd. In addition, distilled water used in these processes was used to formulate the solution and wash the precipitate.

2.2 Preparation of ZnAl-LDH/$ZnCo_2O_4$ materials

2.2.1 Synthesis of $ZnCo_2O_4$

In a typical synthesis procedure, proper amount of $Zn(NO_3)_2\ 6H_2O$ and $Co(NO_3)_3\ 6H_2O$ according to Zn/Co of 1:4 (total cation concentration was 0.05 M) were dissolved in distilled water. After being pretreated with ethyl alcohol, 5 g pine pollen was impregnated in the above precursor solution (50 mL) for 5 h and dried at 40 ^oC for 6 h. Then, the impregnated pine pollen was placed in corundum crucible and calcinated at 300, 400, 500, 600、700 and 800^oC for 1 h, respectively.

2.2.2 Synthesis of ZnAl-LDH/$ZnCo_2O_4$ composite

$Zn(NO_3)_2\ 6H_2O$, urea and $Al(NO_3)_3\ 9H_2O$ were used as starting reagents and ZnAl-LDH/$ZnCo_2O_4$ composite was prepared via the hydrothermal synthesis method. 1.4437 g $Zn(NO_3)_2\ 6H_2O$, 0.6068 g $Al(NO_3)_3\ 9H_2O$ and urea ([urea]/[NO_3^-] molar ratio of 3) were dissolved in 80 ml distilled water with vigorous stirring at room temperature to form a mixed solution. The pH value of the resulting solution was adjusted to 8.5 by drop-wise addition of NaOH solution (2 M). Whereafter, a certain amount of as-prepared $ZnCo_2O_4$ was added to the mixed solution. The resulting reactant was aged in a Teflon-lined stainless-steel autoclave at 120

^{o}C for 10 h. The precipitate was filtered and washed several times with distilled water and ethyl alcohol, and finally dried at 60 ^{o}C for 12 h, which could be denoted as ZnAl-LDH/$ZnCo_2O_4$. In this method, hydrolysis of urea (when the temperature was above 90 ^{o}C) was included two steps, the formation of NH_4CHO, and the fast hydrolysis of cyanate to ammonium carbonate[45]:

$$CO(NH_2)_2 \rightarrow NH_4CNO \quad (1)$$

$$NH_4CNO + 2H_2O \rightarrow 2NH_4^+ + CO_3^{2-} \quad (2)$$

The hydrolysis reactions of urea provide carbonate ions and alkaline condition for the formation of ZnAl-LDH. This alkaline condition is suitable for precipitating a large number of metal hydroxides. The formula for the synthesis of ZnAl-LDH with uera as precipitant is as follows:

$$16OH^- + CO_3^{2-} + 6Zn^{2+} + Al^{3+} + 4H_2O \rightarrow [Zn_6Al_2(OH)_{16}]CO_3^{2-} \cdot 4H_2O \quad (3)$$

After that, the as-synthesized catalyst was placed in muffle furnace and calcinated at 700 ^{o}C for 2 h. The obtained product could be represented as ZnAl-LDO/$ZnCo_2O_4$.

2.3 Characterization

The powder X-ray diffraction patterns of the as-synthesized samples were obtained by using D8-advanced diffractometer (Bruker, AXS) with Cu Ka radiation (40KV, 100mA, λ=0.1540 nm). The samples were scanned for 2θ values ranging from 5^{o} to 80^{o}. Micro-morphologies were characterized by field emission scanning electron microscope (FESEM, FEI QUANTA FEG250, USA) and high resolution transmission electron microscopy (HRTEM; TecnaiF20, Philips, Hillsboro, OR, USA). Fourier transform infrared (FTIR) spectra of the obtained samples were recorded in the spectral range of 4000–500 cm^{-1} on Nicolet 380 FT-IR spectrometer (Thomas Nicolet, USA). Specific surface area of the obtained catalysts was measured by nitrogen adsorption-desorption technique at 77 K using a physisorption analyzer (ASAP2020M+C,

Micrometrics, GA, USA). The method of BJH was used to calculate the pore size distribution. Diffuse reflectance spectroscopy (DRS) was obtained using a Shimadzu UV-3600 spectrometer by using $BaSO_4$ as a reference. The total organic carbon (TOC) concentration was determined using a TOC-analyzer (Shimadzu 5000A).

2.4 Adsorption experiments

In a typical adsorption experiment procedure, 25 mg catalyst was added into 50 mL CR solutions with the initial concentration of 100 mg/L. The mixtures were placed in beaker at room temperature for 0.16, 0.5, 1, 2, 3, 5, 10, 24 and 48 h. The solution and samples were separated by centrifugation at 3500 rpm for 5min. Thereafter, the remaining dyes in supernatant were measured by UV–Vis spectrophotometer (U-3501, Hitachi, Japan) at the wavelength maximum absorbance of 488 nm for CR. The amount of dye adsorbed was calculated based on the formula as given below:[46]

$$q_t = \frac{(C_0 - C_t) \times V}{m} \quad (4)$$

where C_0 (mg/L) is the initial concentration of dyes, C_t (mg/L) is the concentration of dyes at time t (h), V (L) is the volume of dye solution and m (g) is the mass of adsorbent.

2.5 Photocatalytic experiments

Photocatalytic degradation experiments were performed in a photochemical reactor equipped with a 500 W Xenon lamp. In each experiment, 50 mg catalyst was added to 80 mL CR solution (100 mg/L). Before irradiation, the solutions containing the catalyst needed to be placed in the dark for 30 min to reach adsorption equilibrium. During the photocatalytic process, about 10 mL of the suspension was sampled at 10 min intervals of simulated sunlight irradiation. The catalyst was removed from the solution by centrifugation at 3500 rpm for 5 min. Finally, the supernatant

was analyzed by UV–Vis spectrophotometer (U-3501, Hitachi, Japan) at a maximum absorption wavelength of 488 nm for CR. The decomposition efficiency of CR was determined by $D=(1-C_t/C_0)\times 100\%$, where C_0 and C_t are concentration of CR solution at initial and at time t, respectively.

3 Results and discussion

3.1 Structural characterization

Fig. 1a shows the XRD patterns of impregnated pine pollen being calcinated at different temperatures. When the impregnated sample was calcinated at 400-800 ^oC, seven diffraction peaks were observed at 2θ values of about 18.9^o, 31.2^o, 36.8^o, 38.4^o, 44.7^o, 59.2^o and 65.1^o, which could be indexed as (111), (220), (311), (222), (400), (511) and (440) of $ZnCo_2O_4$ (JPCDS, No.23-1390). With the increase of calcination temperature, the diffraction peaks in the patterns became more and more sharp, indicating the grain growth of $ZnCo_2O_4$. Average crystallite size of samples calcined at 400、500、600、700 and 800^oC were about 11.02、11.43、11.68、12.10 and 12.21 nm, respectively, which were calculated by the Scherrer formula[47] using 111、220、311、400、511 and 440 lines. And the standard deviation corresponded to 0.48 nm. And there was no obvious diffraction peak when the calcination temperature was 300 ^oC. In order to select the optimal temperature, we had tested the adsorption and catalytic performance of the samples obtained at different temperatures under the same experimental conditions. The results showed that the performance of the sample increased with the calcinations temperature. However, the performance of the sample obtained at 800 ^oC was similar to that of the sample obtained at 700 ^oC, so we chose 700 ^oC as the optimal temperature based on the consideration of saving resource. In the typical XRD pattern of ZnAl-LDH/$ZnCo_2O_4$ (Fig. 1b-(1)), the main characteristic diffraction peaks of ZnAl-LDH (JPCDS,

No.38-0486) were viewed at 2θ values of approximately 11.6°, 23.3°, 33.8°, 39.1°, 46.6°, 52.8°, 56.1°, 60.1°, 61.4° and 65.4°, which could be assigned to (003), (006), (101), (015), (018), (1010), (0111), (110), (113) and (116) diffraction planes, respectively. The diffraction peaks of $ZnCo_2O_4$ phase were also found in this pattern and no additional peak of another phase was detected. So, it could be regarded that the obtained LDH material was a composite of ZnAl-LDH and $ZnCo_2O_4$ and the combination was a physical process. The XRD pattern of ZnAl-LDO/$ZnCo_2O_4$ composite (Fig. 1b-(2)) revealed that the appearance of the characteristic reflections of $ZnAl_2O_4$ (JPCDS, No.05-0669) could be seen at 2θ values of 18.9°, 31.2°, 36.8°, 44.8°, 59.3° and 65.2°, respectively. At the same time, the characteristic reflections of LDH structure completely disappeared. Furthermore, the characteristic diffraction of $ZnCo_2O_4$ was remained although its reflections were overlapped by broad lines of $ZnAl_2O_4$.

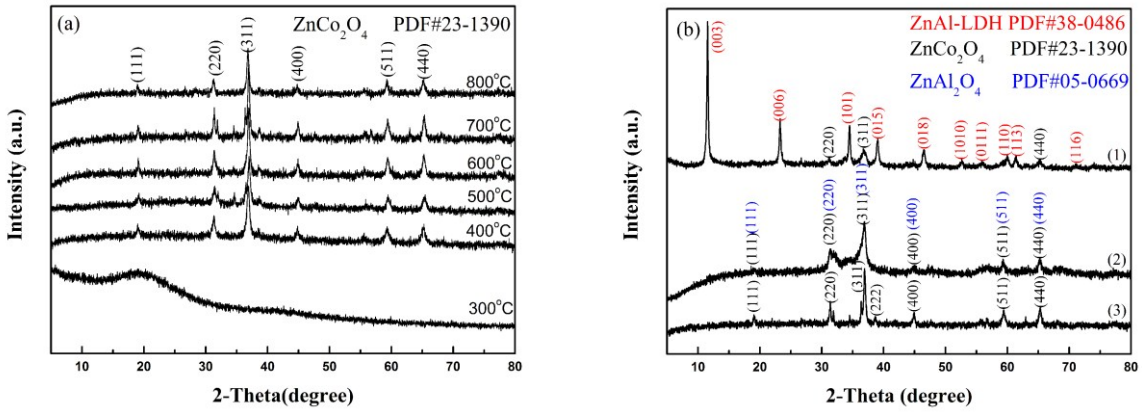

Fig. 1. XRD patterns of the impregnated pine pollen at different calcination temperatures (a), XRD patterns of ZnAl-LDH/$ZnCo_2O_4$ (120 °C, 10 h) (1), ZnAl-LDO/$ZnCo_2O_4$ (700 °C, 2 h) (2) and $ZnCo_2O_4$ (700 °C, 1 h) (3) (b).

Fig. 2 shows the SEM micrographs of the as-prepared samples. The raw pine pollen exhibited a characteristic ellipsoidal structure with two symmetrical hemispherical airbags and the average

size of pollen grains was about 40μm (Fig. 2a-b). $ZnCo_2O_4$ microsphere, which was synthesized by removing the biological template through heat treatment, faithfully inherited the initial surface structure of pine pollen with obvious shrinkage in diameter due to the carbon gasification (Fig. 2c-d). The typical EDS analysis of particles (inset in Fig. 2d) indicated that the as-prepared $ZnCo_2O_4$ mainly contained Zn, Co, O and C, with a Zn/Co molar ratio of ~ 1/4. Fig. 2e exhibits the surface view of the ZnAl-LDH/$ZnCo_2O_4$ samples, which kept the similar ellipsoidal structure with pine pollen, and high magnification (Fig. 2f) shows a large number of LDH crystal films dispersed uniformly on the surface of $ZnCo_2O_4$ substrate. The EDS analysis (inset in Fig. 2f) of the ZnAl-LDH/$ZnCo_2O_4$ structure shows the presence of Zn, Co, Al, O and C, according to the above XRD results, we assumed that the biomorphic structure was a composite of ZnAl-LDH and $ZnCo_2O_4$. After calcination, the resulting product showed similar sheet-like microstructure with ZnAl-LDH/$ZnCo_2O_4$, which mimicked the original macroarchitecture of the pine pollen (Fig. 2g-h). The structure and morphology of as-synthesized samples observed by TEM is shown in Fig. 3. The TEM image (Fig. 3a) implied that the single grain of $ZnCo_2O_4$ exhibited a polygon structure, corresponding to the black dots in the TEM images of ZnAl-LDH/$ZnCo_2O_4$. Fig. 3b-d shows the TEM images of ZnAl-LDH/$ZnCo_2O_4$, in which ZnAl-LDH revealed an irregular sheet-like structure and it was consistent with the results of SEM.

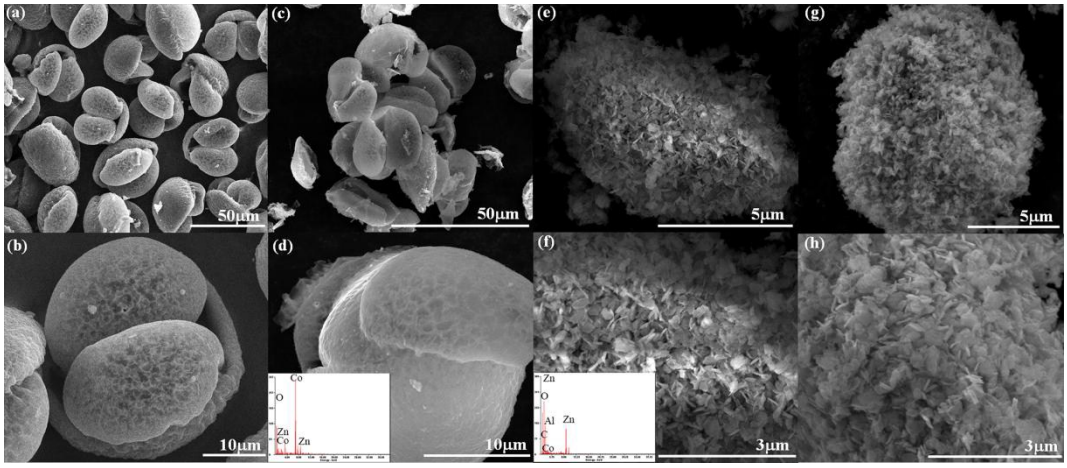

Fig. 2. SEM images of raw pine pollen (a-b), $ZnCo_2O_4$ (700 ^oC, 1h) (c-d), ZnAl-LDH/$ZnCo_2O_4$ (120 ^oC, 10h) (e-f), ZnAl-LDO/$ZnCo_2O_4$ (700 ^oC, 2h) (g-h) at different magnification.

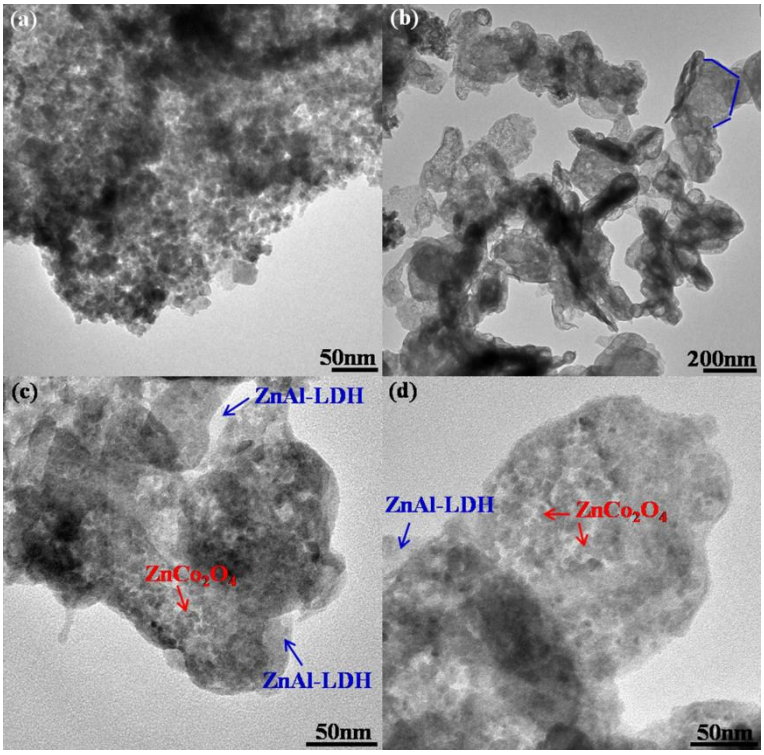

Fig. 3. TEM images of $ZnCo_2O_4$ (700 ^oC) (a) and ZnAl-LDH/$ZnCo_2O_4$ (120 ^oC, 10h) (b-d) at different magnification.

The N_2 adsorption/desorption isotherms and the corresponding BJH pore size distribution curves of the as-synthesized samples are illustrated in Fig. 4. It was observed that the synthesized $ZnCo_2O_4$ sample possessed micro-porous structure with the isotherms were of typical type I, and

the pore size distributions indicated that the samples showed a narrow pore size distribution at about 2 nm. It was confirmed that $ZnCo_2O_4$ had developed porous structure containing micropores and mesopores. The N_2 adsorption/desorption isotherm of the ZnAl-LDH/$ZnCo_2O_4$ presented the typical type IV isotherm with a H3-type hysteresis loop, which indicated the presence of mesopores. While the isotherm of ZnAl-LDO/$ZnCo_2O_4$ exhibited type V with a H3 hysteresis loop. The adsorption at P/P_0=1 was much higher than the mesoporous ZnAl-LDH/$ZnCo_2O_4$ catalyst, indicating the smaller specific area. From the pore size distribution curve of ZnAl-LDO/$ZnCo_2O_4$ obtained by using the BJH method from the adsorption branch of the isotherms, it was found that the pore structure of ZnAl-LDO/$ZnCo_2O_4$ (inset in Fig. 4b) exhibited a large amount of mesopores and some macropores, confirming the hierarchical meso-macroporous structure of our ZnAl-LDO/$ZnCo_2O_4$ catalyst. The specific surface areas, average pore size and total pore volumes of samples are listed in Table 1. The lower specific surface area of ZnAl-LDO/$ZnCo_2O_4$ composite was probably due to the expansion of pore size caused by the further removal of carbon during the calcination process.

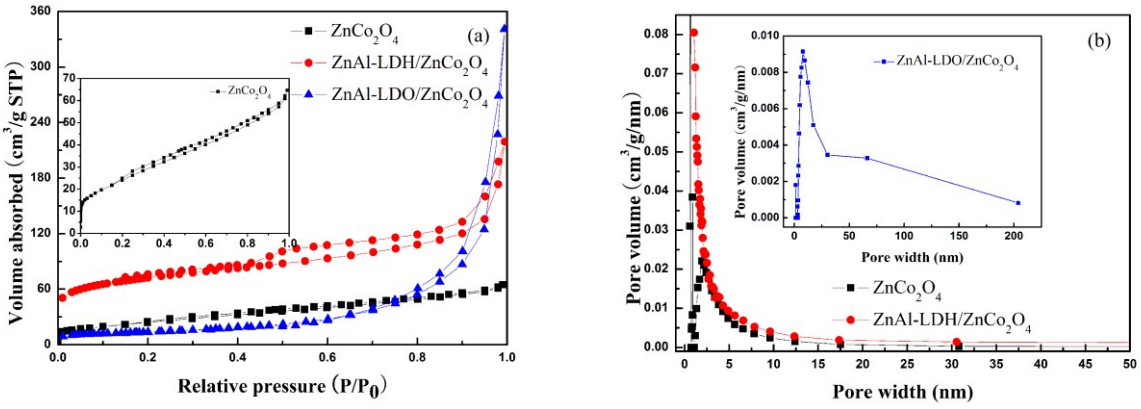

Fig. 4. Nitrogen adsorption and desorption isotherms (a) and corresponding BJH pore size distribution curves of the samples (b).

Table1 Textural properties of samples.

Sample	specific surface areas (m^2/g)	average pore size (nm)	total pore volumes (cm^3/g)
$ZnCo_2O_4$	89.73	0.51	0.1000
ZnAl-LDH/$ZnCo_2O_4$	257.79	5.26	0.3393
ZnAl-LDO/$ZnCo_2O_4$	48.26	43.75	0.5274

Fig. 5a shows the FTIR spectra of impregnated pine pollen being calcinated at different temperatures. The broad band at 3450 cm^{-1} was attributed to O-H stretching. When the calcination temperature was 300 ^oC, the peaks at 2930 cm^{-1} and 2850 cm^{-1} were generated by the stretching vibrations of C-H in aliphatic, indicating the biological template had not been fully removed. When the calcination temperature was above 300 ^oC, the bands at 667 and 582 cm^{-1} belonged to the Co-O stretching vibrations appeared, implying the formation of $ZnCo_2O_4$. With the calcination temperature increased, the characterristic peaks at 667 and 582 cm^{-1} became more and more sharp, indicating the grain growth of $ZnCo_2O_4$. In the FTIR spectrum of ZnAl-LDH/$ZnCo_2O_4$ (shown in Fig. 5b), the broad and strong band centered at 3440 cm^{-1} was assigned to the O–H stretching vibration of surface and interlayer water molecules. The peak near 1620 cm^{-1} could be contributed by the bending vibration of interlayer water molecules. The narrow adsorption at 1380 cm^{-1} was ascribed to the ν_3 stretching mode of the interlayer carbonate anions in a symmetric environment, and the band close to 877 cm^{-1} was resulted from the ν_2 mode of the interlayer carbonate group.[48] Two bands around 553 and 779 cm^{-1} were due to the translation mode of Al–OH.[39] Moreover, the peaks at 677 and 588 cm^{-1} represented the stretching vibration of Co-O were also found in the

spectrum, which manifested the presence of $ZnCo_2O_4$. After calcination, the absorption peak at 1380 cm^{-1} (due to the stretching vibration of CO_3^{2-}) became considerably weak, the peaks in the low-frequency region corresponded to the lattice vibration modes such as the vibrations of Al-OH at 553 cm^{-1} and 779 cm^{-1} disappeared and the bands assigned to characteristic peaks of spinel structure at 667 cm^{-1} and 588 cm^{-1} were slightly broadened. From the FTIR spectra of ZnAl-LDH/$ZnCo_2O_4$ composite after calcinations (Fig. 5b), we can see that the bands at 3440 and 1620 cm^{-1} corresponded to water molecules were weakened to some extent, but still survived to the thermal treatment at 700 ^oC. This may due to the fact that the environment humidity is large and water can be adsorbed from the atmosphere.

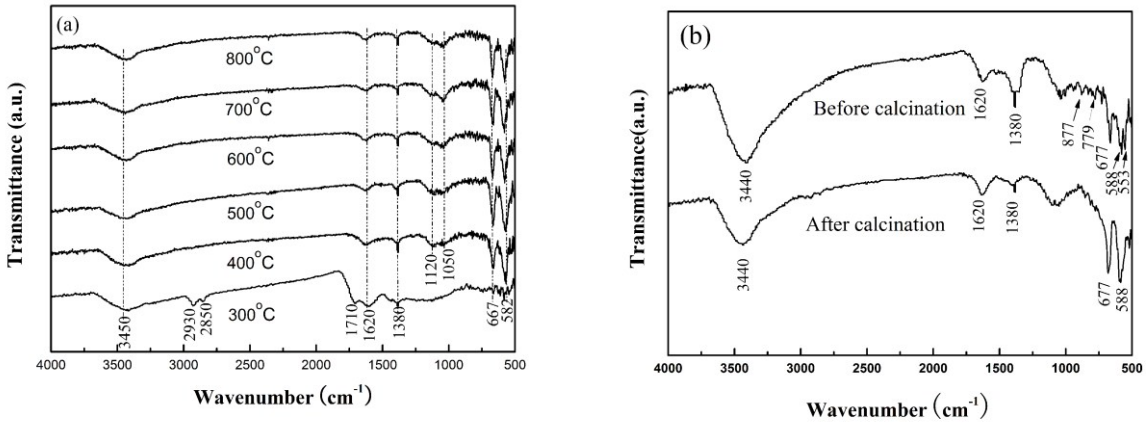

Fig. 5. FTIR spectra of the impregnated pine pollen being calcinated at different temperatures (a), ZnAl-LDH/$ZnCo_2O_4$ composite before and after calcinations (b).

The light absorbance of the as-prepared samples was evaluated by the UV–Vis diffuse reflection absorption spectra and the results are shown in Fig. 6a. The pure $ZnCo_2O_4$ absorbance was the whole waveband. Apparently, pure ZnAl-LDO only had absorbance in the UV region, but its adsorption edge was widened when it was composited with $ZnCo_2O_4$. As shown in Fig. 6a, the adsorption of the porous ZnAl-LDO/$ZnCo_2O_4$ composites showed the enhanced absorption at

visible region. By comparing LDO with LDO/$ZnCo_2O_4$, it could be clearly seen that the performance of UV-Vis absorption was apparently enhanced as combined with $ZnCo_2O_4$. According to the results of UV-Vis, it could be assumed that the combination with $ZnCo_2O_4$ successfully enhanced the light absorbance of ZnAl-LDO into visible region. The optical band gap of the as-prepared catalysts was determined by the following equation using the data of optical absorption versus wavelength near the band edge.[49]

$$(\alpha h\upsilon)^n = A\left(h\upsilon - E_g\right) \quad (5)$$

where α, υ, A and Eg are absorption coefficient, light frequency, constant and band gap, respectively. In the equation, n decides the characteristics of the transition in a semiconductor, that is, a direct transition for n = 2 and an indirect transition for n = 1/2. Fig. 6b shows the band gap energy of LDO calculated by the equation was about 3.82 eV. The band gap energies of $ZnCo_2O_4$ microspheres were calculated to be 1.62 and 2.62 eV, which was in accordance with the work by Guo.[26]

The general description of the electron configuration in the spinel structure of $ZnCo_2O_4$ is the tetrahedral high spin Zn^{2+} (e^4_g t^6_{2g}) with octahedral low spin Co^{3+} (t^6_{2g}).[26] The band structure of $ZnCo_2O_4$ is usually defined by taking O 2p orbital as the valence band and Co 3d orbital as the conduction band.[49] Based on the band gad energies calculated from the UV-Vis absorption spectrum, a simplified electronic band structure of $ZnCo_2O_4$ was proposed and illustrated in Fig. 7. It can be assumed that three kinds of photoexcitation of electrons may take place with respect to the energy of incident photons: (1) from O 2p to Co 3d-e_g; (2) from O 2p to Co 3d-t_{2g}; and (3) from Co 3d-t_{2g} to Co 3d-e_g.[26] The photoexcitation (1) and (2) correspond to two direct energy bandgaps of $ZnCo_2O_4$, respectively, which are 2.62 and 1.62 eV. The photoexcitation (3) may play

an important role in the photoexcitation and photocatalytic activity.[50]

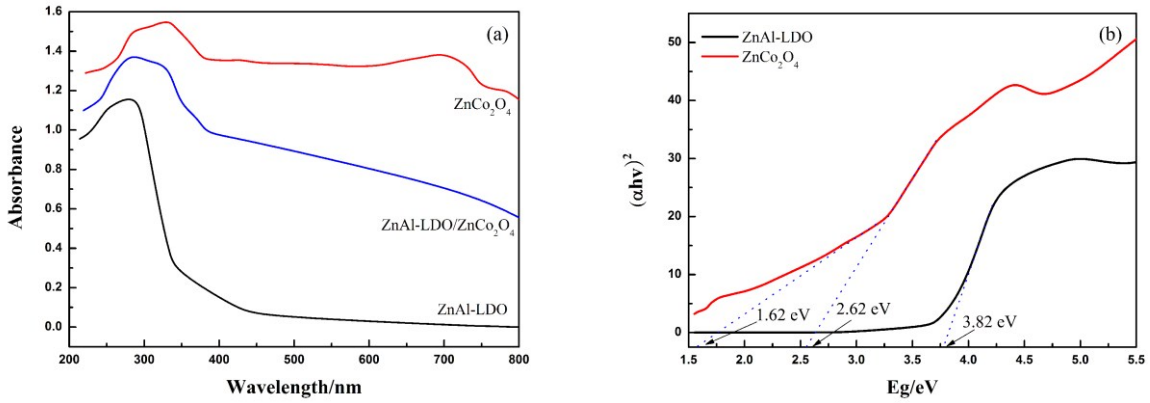

Fig. 6. UV-Vis spectra of the as-prepared samples (a) and the calculated band energies (b).

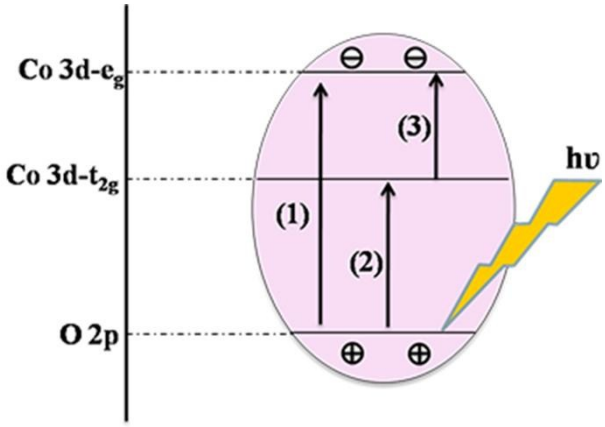

Fig. 7. Schematic illustration of the electronic band structure of $ZnCo_2O_4$

According to the results of aforementioned XRD, SEM, TEM and FTIR results, the scheme illustration of the formation of ZnAl-LDH/$ZnCo_2O_4$ composite is proposed and schematically illustrated in Fig. 8. The formation process may be summarized four stages, that is, ions anchoring, nucleation and growth, template removal and hydrothermal crystallization. Initially, under heat treatment conditions, collision and combination of the precursor ions (Zn^{2+}, Co^{3+}) led to the formation of $ZnCo_2O_4$ nanocrystals. Then, tiny $ZnCo_2O_4$ nanocrystals began to nucleate and grow, and pollen template was gradually thermal decomposed during calcinations, leaving the $ZnCo_2O_4$ self-assembly structures with pine pollen morphology. Finally, ZnAl-LDH, which was generated

by hydrothermal reaction, and $ZnCo_2O_4$ precursor combined through intermolecular forces.

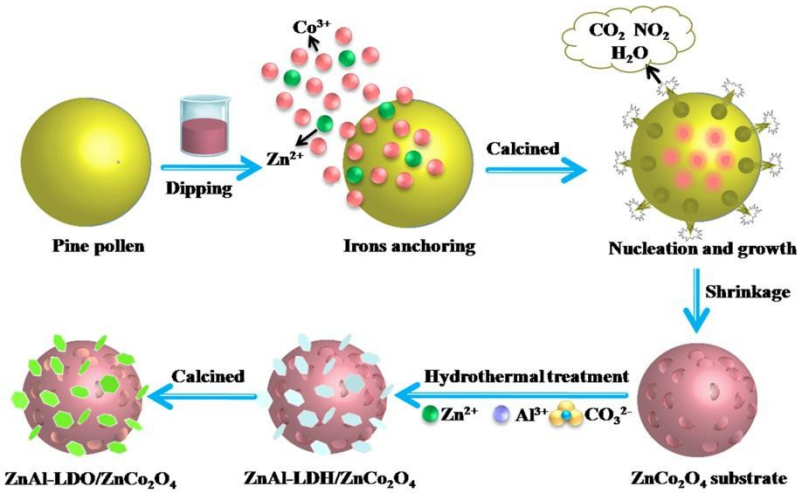

Fig. 8. Schematic illustration of the synthesis of pollen-like ZnAl-LDH/$ZnCo_2O_4$ and its derived metal oxides

3.2 Adsorption performance

Congo red was chosen as the target contaminant to study the catalytic behavior of as-synthesized samples. Since the biomorphic $ZnCo_2O_4$ and LDH both can be used as adsorbent, the catalytic degradation becomes a complex process wherein catalysis and adsorption may take place at the same time. Therefore, it is important to study the adsorption performance of the composite.

The effects of contact time on CR adsorption by different adsorbents synthesized using pollen as biotemplate are illustrated in Fig. 9a. Both adsorption amount of CR increased rapidly in the initial adsorption stage and then increased slowly until the equilibrium was attained at 48 h. Compared with photocatalytic degradation, the adsorption of CR onto as-synthesized catalyst was a slower process, so it needed longer time to reach equilibrium. The equilibrium adsorption capacity of ZnAl-LDH/$ZnCo_2O_4$ and its derived metal oxides towards CR were up to 142.45 and 268.81 mg/g, respectively. However, the adsorption capacity of $ZnCo_2O_4$ substrate and pure ZnAl-LDH were 52.80 and 139.66 mg/g, respectively, which indicated that the presence of $ZnCo_2O_4$ substrate did

not affect the adsorption ability of LDH. The effects of contact time on CR adsorption by the same materials synthesized without biotemplate were also discussed (Fig. 9b). Compared with the samples synthesized using pine pollen as template agent, the same materials synthesized without template exhibited weaker adsorption performance. This could be ascribed to the porous pollen-like structure can provide more available adsorption sites during the adsorption process.

Pseudo-second-order model of Ho and McKay[51] was adopted by many to describe the kinetics of dye molecules:

$$\frac{t}{q_t} = \frac{1}{K_2 q_e^2} + \frac{t}{q_e} \quad (6)$$

where q_t and q_e are the adsorption capacity (mg/g) at time t and at equilibrium conditions, respectively. K_2 is the rate constant of pseudo-second order model (g /mg· h).

Table 2 shows the relevant parameters of the kinetic models. Based on the parameters, high values of correlation coefficient R^2 indicated that pseudo-second-order kinetic model was suitable for describing the adsorption behavior of CR onto the adsorbents in this study. The graphs of the adsorbed CR mass (q_t) versus different initial concentrations C_0 are shown in Fig. 9c. It was observed that the adsorption capacity increased with concentration and maintained near 209 and 349 mg/g for ZnAl-LDH/$ZnCo_2O_4$ and its derived metal oxides, respectively.

The surface charge of adsorbent is affected by the pH values of dye solution, so it is very important to investigate its influence on adsorption process. The effect of solution pH on CR removal is demonstrated in Fig. 9d, adsorption capacities of ZnAl-LDH/$ZnCo_2O_4$ and its derived metal oxides both decreased with the increase of pH values, indicating the influence of pH on adsorption process is significant. The influence of solution pH on adsorption of CR could be explained by the changes in surface charge of adsorbent with the varied solution pH values. Higher

CR adsorption quantities under strong acidic conditions could be ascribed to the fact that strong electrostatic attraction existed between the positively charged surface of adsorbent and the negatively charged sulfonic acid group of CR. With the increment of solution pH values, the number of positively charged sites on the surface of adsorbent decreased and negatively charged sites increased, resulting in the decrement in adsorption quantities. Under alkaline condition, the negatively charged surface was not conducive to the adsorption of dye due to the electrostatic repulsion. As a result, the electrostatic repulsion between adsorbent and adsorbate was the main factor under alkaline condition.

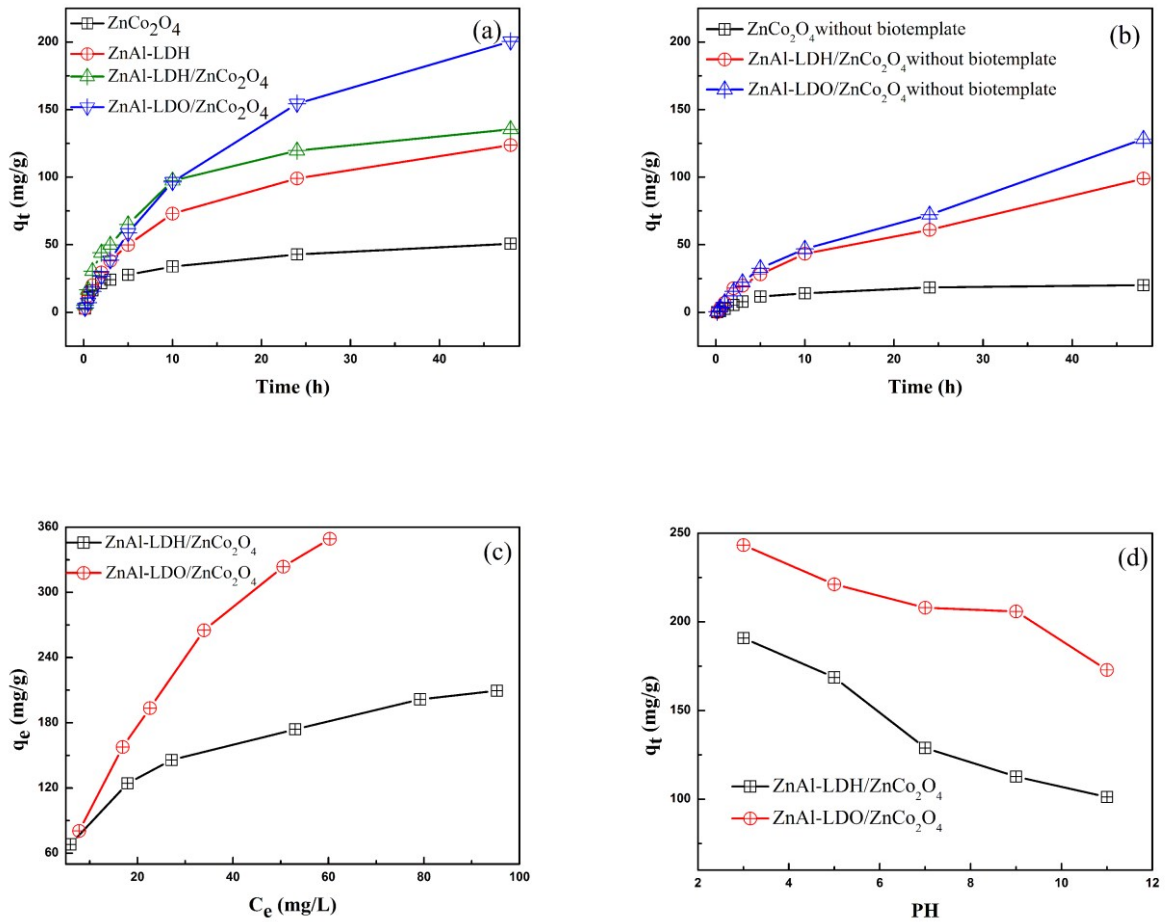

Fig. 9. Effect of contact time on CR removal by different adsorbents synthesized using pollen as template (a) (100 mg/L CR, 50 mL CR, 0.5 g/L catalyst), effect of contact time on CR removal by the same materials

synthesized without biotemplate (b) (100 mg/L CR, 50 mL CR, 0.5 g/L catalyst), adsorption isotherms of CR on different adsorbents (c) (50 mL CR, 0.5 g/L catalyst), effect of initial pH values of dye solution on adsorption of CR onto ZnAl-LDH/$ZnCo_2O_4$ and its derived metal oxides (d) (100 mg/L CR, 50 mL CR, 0.5 g/L catalyst).

Table2 Kinetic constants for CR adsorption onto different adsorbents with biotemplate analyzed by pseudo-second-order model

Sample	$q_{e,exp}$(mg/g)	$q_{e,cal}$(mg/g)	K_2(g/mgh)	R^2
$ZnCo_2O_4$	50.69	52.80	0.0054	0.9921
Pure ZnAl-LDH	123.77	139.66	0.0009	0.9901
ZnAl-LDH/$ZnCo_2O_4$	135.47	142.45	0.0008	0.9970
ZnAl-LDO/$ZnCo_2O_4$	198.46	268.81	0.0002	0.9900

3.2.1 Adsorption mechanism

In order to better discuss the adsorption mechanism, infrared spectrum analysis of the as-synthesized adsorbents after dye adsorption was carried out (Fig. 10a). In spectra of CR (shown in Fig. 10a-(1)), the band at 3460 cm^{-1} was caused by N-H stretching, the peaks at 1120 and 1040 cm^{-1} were ascribed to S-O stretching of the sulfonate group in CR.[52] By comparing the FTIR spectra of ZnAl-LDH/$ZnCo_2O_4$ before (Fig. 5b) and after (Fig. 10a-(2)) dye adsorption, the peak shift from 1380 cm^{-1} to 1360 cm^{-1} could be ascribed to the intercalation of -SO_3^- of CR.[53] Moreover, in the FTIR spectra of ZnAl-LDH/$ZnCo_2O_4$ (Fig. 10a-(2)) after dye adsorption, the characteristic band of -SO_3^- near 1040 cm^{-1} was very clear, which was a clear evidence of the adsorption of CR onto ZnAl-LDH/$ZnCo_2O_4$ and ZnAl-LDH/$ZnCo_2O_4$. In conclusion, the adsorption of CR dyes onto ZnAl-LDH/$ZnCo_2O_4$ composite could be speculated to occur in two steps (Fig. 11). Firstly, adsorption occurred at the surface of the adsorbent through electrostatic attraction for CR. Then,

followed by anion exchange, the interlayer anion of CO_3^{2-} was subsequently substituted for $-SO_3^-$ of CR dyes.

For the case of ZnAl-LDO/$ZnCo_2O_4$, it was found that, after CR removal with LDO at initial CR concentration of 100 mg/L, the LDO material experienced structural reconstruction (Fig. 10b-(3)). And no characteristic diffraction peaks of the hydroxide layered structure was found in the XRD patterns of LDO after adsorption of CR with a contact time of 150 min (Fig. 10b-(2)), which indicated the reconstruction process need longer time. However, no significantly difference in the basal spacing was observed (7.56 Å of LDO after sorption of CR (100 mg/L) and 7.60 Å of ZnAl-LDH (Fig. 1b)), suggesting that CR was adsorbed on the external surface of the ZnAl-LDO/$ZnCo_2O_4$ rather than intercalated between the interlayer. For the recombined LDH, in addition to the carbonate ions, some hydroxy anions in water may also intercalate in the interlayer region of LDH (since the basal spacing of OH^- intercalated LDH was 7.30 Å). The FTIR analysis from Fig. 10a further verified the successful adsorption of CR by the increase in the two bands related to SO_3^- at 1120 and 1050 cm^{-1} after CR adsorption. We presume the adsorption mechanism was mainly the surface sorption. Interestingly, the adsorption capacity of LDO was much larger than that of LDH, it could be attributed to the following three reasons: (1) strong interaction of CO_3^{2-} and the layers of LDH can prevent the anion exchange to some extent; (2) after calcinations, the obstacle anions (mainly CO_3^{2-}) were released from the precursor, producing more active sites for CR adsorption[54] and (3) macroporous networks of LDO can provide more accessible diffusion pathways for adsorbates[55].

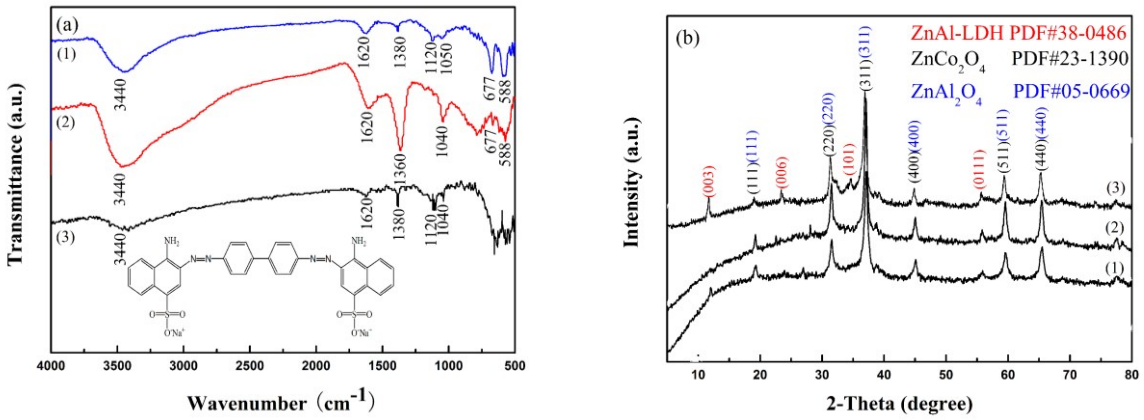

Fig. 10. (a) FTIR spectra of ZnAl-LDO/$ZnCo_2O_4$ (1) and ZnAl-LDH/$ZnCo_2O_4$ (2) after adsorption of CR (3) (Inset: CR structure), (b) XRD patterns of ZnAl-LDO/$ZnCo_2O_4$ after adsorption of CR (0 mg/L) for 48 h (1), 100 mg/L for 150 min (2) and 100mg/L for 48 h (3).

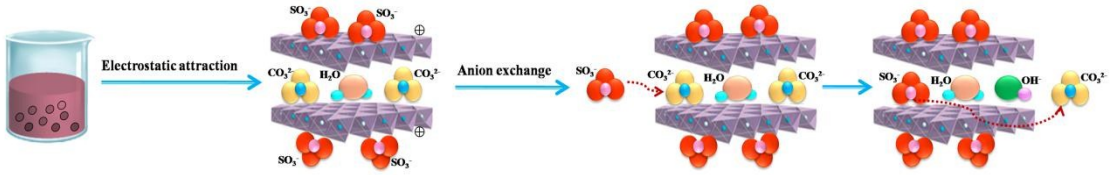

Fig. 11. Possible adsorption mechanism diagram of CR onto ZnAl-LDH/$ZnCo_2O_4$

3.3 Photocatalytic performance

3.3.1 Photocatalytic activity and stability

The photocatalytic activities of as-synthesized samples under simulated sunlight irradiation are shown in Fig. 12a. Under the dark conditions, the concentration of CR dye had tiny changes for a long time in the presence of catalysts. At the same time, adsorptive action could concentrate dyes on the surface of the catalyst, which can facilitate the catalytic degradation of CR. It was obvious that the resulting calcination product (ZnAl-LDO/$ZnCo_2O_4$) exhibited the best photocatalytic performance when the reaction was performed under simulated sunlight for 120 min. In order to

highlight the advantages of biological templates, the photocatalytic activities of same materials synthesized without template were also evaluated. As shown in Fig. 12b, both samples synthesized without template showed lower photocatalytic activities than the same materials synthesized using pollen as template agent. This may be attributed to the micro-ellipsoidal structure of pollen template could provide the reactant medium and expedite the mass transportation during the catalysis process.

Except photocatalytic activity, the stability of catalysts is another important factor in their practical applications. To analyze the effect of recycle times on CR removal, the used catalysts were calcined again and reused in the new experiments with the fresh CR solution to assess their cycle performance. As shown in Fig. 12c, the first 3 cycles contained the results from the catalysts of $ZnCo_2O_4$ and ZnAl-LDO/$ZnCo_2O_4$, while the 4th and the 5th cycle contain only results from the ZnAl-LDO/$ZnCo_2O_4$ catalyst of this contribution. After 3 cycling runs, differences in the kinetic curves between $ZnCo_2O_4$ and ZnAl-LDO/$ZnCo_2O_4$ were observed for the whole process, meaning that the photocatalytic activity of ZnAl-LDO/$ZnCo_2O_4$ was significantly different from that of $ZnCo_2O_4$. Even after 5 cycling runs, ZnAl-LDO/$ZnCo_2O_4$ still given 79% degradation rate of CR after 120 min simulated sunlight irradiation, which indicated that ZnAl-LDO/$ZnCo_2O_4$ composite can serve as an effective and recyclable photocatalyst.

3.3.2 Kinetic modeling

The degradation kinetic of CR was examined by following the pseudo first-order kinetic equation:[56]

$$-\ln\left(\frac{C_t}{C_0}\right) = k_{app}\, t \qquad (7)$$

where C_0 and C_t are the dye concentrations at initial and at time t, respectively, k_{app} is the apparent

reaction rate constant. The values of k_{app} (min^{-1}) are listed in Table 3. Compared with $ZnCo_2O_4$ substrate and ZnAl-LDH/$ZnCo_2O_4$ composite, ZnAl-LDO/$ZnCo_2O_4$ showed higher photocatalytic activity, this was represented by larger value of k_{app}.

Fig. 12d shows the UV-vis spectra of CR treated by ZnAl-LDO/$ZnCo_2O_4$ at different simulated sunlight irradiation time intervals. The spectrum of the raw CR solution had two prominent peaks at 498 and 345 nm. Among them, the peak at 498 nm was attributed to the chromophore structure next to azo bonds and the band in the ultraviolet range located at nearly 345 nm was corresponding to naphthalene rings in the mother molecule.[57] During the photodegradation process, these adsorption peaks diminished vary fast and nearly completely disappeared after 40 min simulated sunlight irradiation, which indicated that the breakdown of chromophore responsible for the characteristic color of CR.

Table 3 Kinetic constants for CR degradation onto different catalysts with bio-template analyzed by pseudo-first-order model

catalyst	k (min^{-1})	R^2
$ZnCo_2O_4$	0.0147	0.9896
ZnAl-LDH/$ZnCo_2O_4$	0.0041	0.9906
ZnAl-LDO/$ZnCo_2O_4$	0.0212	0.9883

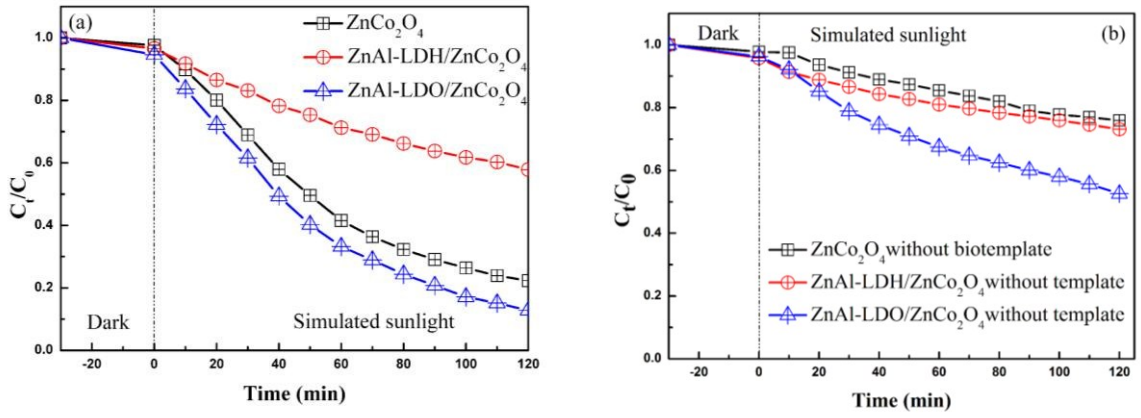

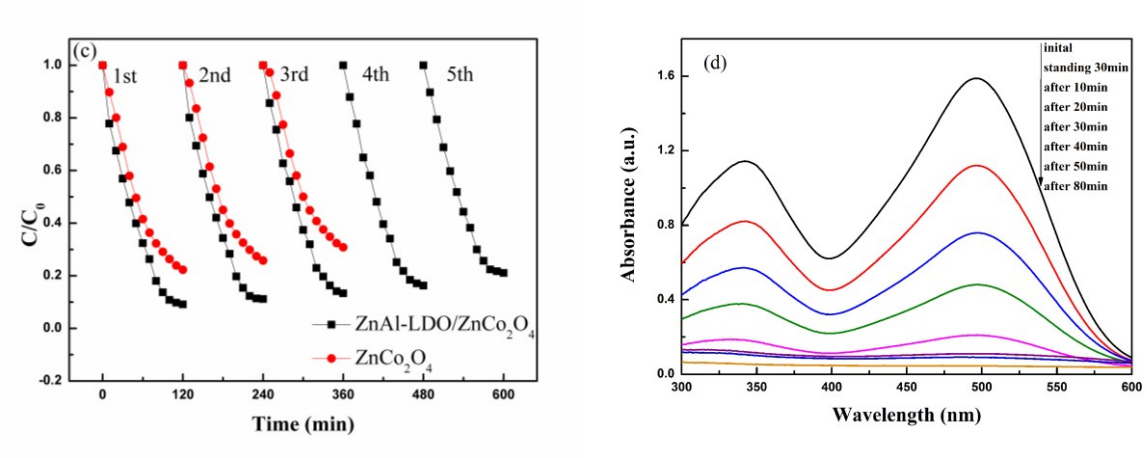

Fig. 12. Degradation curves of CR by different catalysts with biotemplate under simulated sunlight irradiation (a), degradation curves of CR by the catalysts without biotemplate under simulated sunlight irradiation (b), cycling runs of ZnAl-LDO/$ZnCo_2O_4$ and $ZnCo_2O_4$ for CR degradation under simulated sunlight irradiation (c), UV-vis spectra of CR solutions during degradation process (100 mg/L CR, 80 mL CR, 0.625 g/L catalyst).

3.3.3 Kinetics of TOC disappearance

It has been widely reported that some degradation products could be more toxic than the original dye[58]. Before the discharge of sewage, if the dye components are mineralized by catalysts, it is highly desirable[59]. In order to evaluate the degradation of organic compounds in the process of photocatalysis, total organic carbon (TOC) concentration was analyzed. Apparent mineralization of CR was observed in the present work, and the TOC removal of CR was up to 64.96% after 120 min of simulated sunlight irradiation when the ZnAl-LDO/$ZnCo_2O_4$ catalyst was used. Only 38.58% of TOC removal was measured when using the as-prepared $ZnCo_2O_4$ (Fig. 13). This indicated that the photodegradation with the prepared ZnAl-LDO/$ZnCo_2O_4$ catalysts was not only decomposition, but also a deep oxidation process to mineralize organic molecules into inorganic ones such as SO_4^{2-}, NO_3^-, CO_2 and H_2O. The formula of CR oxidation is as follows:

$$C_{32}H_{22}N_6O_6S_2^{2-} + {}^{91}/_{2}\,O_2 \rightarrow 32CO_2 + 6NO_3^- + 2SO_4^{2-} + 8H^+ + 7H_2O \quad (8)$$

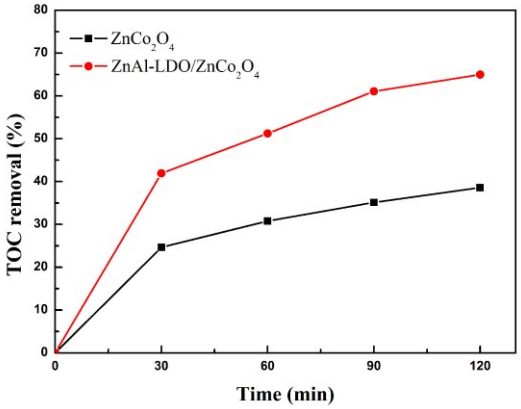

Fig. 13. TOC removal kinetics for the as-prepared catalysts.

3.3.4 Photocatalytic mechanism

A tentative photo-degradation mechanism of the ZnAl-LDO/$ZnCo_2O_4$ is schematically shown in Fig. 14. Generally, the photocatalytic property is closely related with the band gap structure of semiconductor. The condution band-edge could be forecasted by the following empirical formula:[60]

$$E_{CB}^0 = \chi - E^C - 0.5E_g \quad (9)$$

where χ is the absolute electronegativity of the semiconductor (χ is 5.95 and 5.48 eV for $ZnCo_2O_4$ and $ZnAl_2O_4$, respectively). E^C is the energy of free electrons on the hydrogen scale (4.5 eV) and E_g is the band gap energy of the semiconductor. Based on Eq. (9), the conduction band values of $ZnCo_2O_4$ and ZnAl-LDO were 0.64 and -0.93 eV, respectively. $ZnCo_2O_4$ and LDO can be both excited and produce photogenerated electron-hole pairs under simulated sunlight irradiation. When the photon energy was equal to or higher than the band gap of $ZnCo_2O_4$ (LDO), electrons (e^-) in the valence band (VB) would be excited to the conduction band (CB), and generating the same

amount of holes (h^+) in the VB. Since the difference of energy level between VB and CB in $ZnCo_2O_4$ and LDO, the photo-generated electrons in $ZnCo_2O_4$ immigrate to the conduction band of LDO and the holes at the valence band of LDO would shift to that of $ZnCo_2O_4$, which effectively prevented the recombination of electrons and holes. Subsequently, electrons could be easily captured by O_2 molecules (adsorbed on the catalyst surface) to produce $\cdot O^{2-}$ radical. Meanwhile, photo-generated holes in $ZnCo_2O_4$ could be also trapped by the immanence H_2O molecules to generate $\cdot OH$ radicals. These active substances could oxidize organic chemicals into inorganic small molecules, such as CO_2 and H_2O.

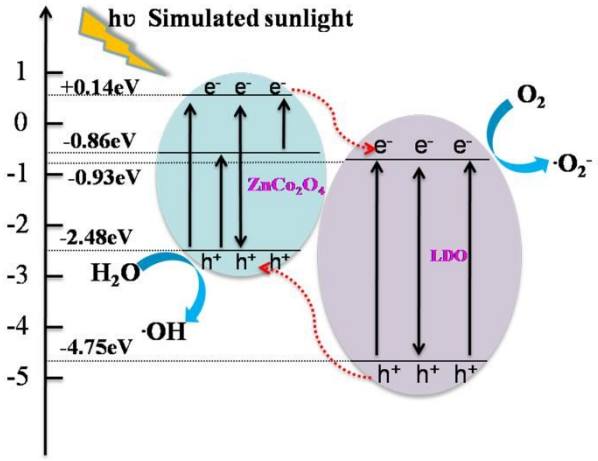

Fig. 14. Possible photocatalytic mechanism scheme of ZnAl-LDO/$ZnCo_2O_4$.

4 Conclusion

In summary, ZnAl-LDH/$ZnCo_2O_4$ composite was synthesized by using pine pollen as biological template. The obtained $ZnCo_2O_4$ substrate, ZnAl-LDH/$ZnCo_2O_4$ composite, and its derived metal oxides all mimicked the original macroarchitecture of the pine pollen. Layered ZnAl-LDH dispersed uniformly on the surface of the support of $ZnCo_2O_4$ ellipsoid. Consequently,

a novel biomorphic composite was prepared, characterized and applied for removing CR dyes from wastewater. The adsorption of CR onto the obtained samples depended upon the time of contact, the values of solution pH and the initial concentrations of CR solution, which followed the pseudo-second-order kinetic model. In addition, under the conditions of 100 mg/L and 80 mL CR solution, 50 mg catalyst dose and Xenon lamp power 500 W, the calcined sample showed better photocatalytic activity and 91% degrading efficiency of CR could be obtained after 120 min simulated sunlight irradiation. Kinetics studies showed that the degradation of CR fitted the pseudo first-order kinetic model. The special hierarchical structure of the materials can effectively improve the adsorption and photocatalytic performance of the obtained sample.

Acknowledgements

This work was supported by the National Natural Science Foundation of China (Grant No.51172095 and No.61102006).

References

[1] V.K. Gupta, Suhas, *J. Environ. Manage.*, 2009, **90**, 2313–2342.

[2] D. Shen, J. Fan, W. Zhou, B. Gao, Q. Yue, Q. Kang, *J. Hazard. Mater.*, 2009, **172**, 99–107.

[3] M. Rafatullaha, O. Sulaimana, R. Hashima, A. Ahmad, *J. Hazard. Mater.*, 2010, **177**, 70–80.

[4] S.Y. Dong, J.L. Feng, M.H. Fan, Y.Q. Pi, L.M. Hu, X. Han, M.L. Liu, J.Y. Sun and J.H. Sun, *RSC Adv.*, 2015, **5**, 14610-14630.

[5] J.P. Guin, Y. K. Bhardwaj, D. B. Naik and L. Varshney, *RSC Adv.*, 2014, **4**, 53921-53926.

[6] D.W. Chen, A.K. Ray, *Chem. Eng. Sci.*, 2001, **56**, 1561-1570.

[7] A. Fujishima, K. Honda, *Nature.*, 1972, **238** (5358), 37–38.

[8] L. Ren, Y.Z. Li, J.T. Hou, X.J. Zhao, C.X. Pan, *ACS. Appl. Mater. Inter.*, 2014, **6**, 1608−1615.

[9] T.J. Zhu, J. Li, Q.S. Wu, ACS. *Appl. Mater. Inter.*, 2011, **3**, 3448–3453.

[10] P.S.M. Gharavi, M.R. Mohammadi, Sol. *Energ. Mat. Sol. C.*, 2015, **137**, 113–123.

[11] X.N. Fei, F.D. Li, L.Y. Cao, G.Z. Jia, M. Zhang, *Mat. Sci. Semicon. Proc.*, 2015, **33**, 9–15.

[12] G. Xiao, X. Zhang, W.Y. Zhang, S. Zhang, H.J. Su, T.W. Tan, *Appl. Catal. B: Environ.*, 2015, **170-171**, 255–262.

[13] L. Gomathi Devi and R. Kavitha, *RSC Adv.*, 2014,**4**, 28265-28299.

[14] S. Dwivedi, R. Sharma, Y. Sharma, Opt. Mater., 2014, **37**, 656–665.

[15] H. Zhang, X.Y. Cheng, R.Z. Sun, Y.Z. Guan, Y.W. Liu, C.G. Yin, X.S. Liang, G.Y. Lu, *Sensor. Actuat. B-Chem.*, 2014, **198**, 26–32.

[16] J. Ghose, K.S.R.C. Murthy, *J. Catal.*, 1996, **162**, 359–360.

[17] S.W. Cao, Y.J. Zhu, G.F. Cheng, Y.H. Huang, *J. Hazard. Mater.*, 2009, **171**, 431–435.

[18] J. Zeng, M.D. Xin, K.W. Li, H. Wang, H. Yan, W.J. Zhang, *J. Phys. Chem. C.*, 2008, **112**, 4159-4167.

[19] M.B. Ali, F. Barka-Bouaifel, H. Elhouichet, B. Sieber, A. Addad, L. Boussekey, M.Férid, R. Boukherroub, *J. Colloid Interface Sci.*, 2015, **457**, 360–369.

[20] R. Sarkari, C. Anjaneyulu, V. Krishna, R. Kishore, M. Sudhakar, A.Venugopal, *Catal. Commun.*, 2011, **12**, 1067–1070.

[21] B. Cui, H. Lin, Y.Z. Liu, J.B. Li, P. Sun, X.C. Zhao, C.J. Liu, *J. Phys. Chem. C.*, 2009, **113**, 14083–14087.

[22] D.F. Wang, Z.G. Zou, J.H. Ye, *Chem. Phys. Lett.*, 2003, **373**, 191–196.

[23] H.W. Chen, A.F. Liu, X.L. Zhang, J.B. Mu, Y.M. Bai, J.X. Hou, *Ceram. Int.*, 2015, **41**, 7556–7564.

[24] W.B. Fu, X.L. Li, C.H. Zhao, Y. Liu, P.Zhang, J.Y. Zhou, X.J. Pan, E.Q. Xie, *Mater. Lett.*, 2015, **149**, 1–4.

[25] F.J. Sun, X.G. Li, L.P. Liu, J. Wang, Sensor. *Actuat. B-Chem.*, 2013, **184**, 220–227.

[26] H.X. Guo, J.H. Chen, W. Weng, Q.X. Wang, S.X. Li, *Chem. Eng. J.*, 2014, **239**, 192–199.

[27] B. Cui, H. Lin, X.C. Zhao, J.B. Li, W.D. Li, *Acta Phys-Chem. Sin.*, 2011, **27**, 2411–2415.

[28] P. Song, H.H. Zhang, D. Han, J. Li, Z.X. Yang, Q. Wang, *Sensor. Actuat. B-Chem.*, 2014, **196**, 140–146.

[29] Y.M. Liu , H. Lv, J.Y Hu, Z.J. Li, *Mater. Lett.*, 2015, **139**, 401–404.

[30] X.D Ye, Q. Yang, Y.F. Zheng, W.M. Mo, J.G. Hu, W.Z. Huang, *Mater. Res. Bull.*, 2014, **51**, 366–371.

[31] R. Selvakumar, N. Seethalakshmi, P. Thavamani, R. Naidu and M. Megharaj, *RSC Adv.*, 2014, **4**, 52156-52169.

[32] J. He, Y.F. Zhao, D.B. Xiong, W. Ran, J. Xu, Y.Q. Ren, L. Zhang, Y.F. Tang, F.M. Gao, *Mater. Lett.*, 2014, **128**, 117–120.

[33] Y. M, Q.L. Wei, R.W. Ling, F.K. An, G.Y. Mu, Y.M. Huang, *Micropor Mesopor Mat.*, 2013, **165**, 177–184.

[34] X.J. Fan, X.Q. Song, X.H. Yang, L.X. Hou, *Mater. Res. Bull.*, 2011, **46**, 1315–1319.

[35] J.C. Qian, Z.G. Chen, C.B. Liu, X.W. Lu, F. Wang, M.M. Wang, *Mat. Sci. Semicon. Proc.*, 2014, **25**, 27–33.

[36] L. Yue, J.B. Guo, Q. Yang, X. Luo, J. Lian, J.L. Yang, L. Wang, *Mater. Lett.*, 2015, **157**, 225–227.

[37] D. Basu, A. Das, K.W. Stöckelhuber, U. Wagenknecht, G. Heinrich, *J. Prog. Poly. Sci.*, 2014, **39**, 594–626.

[38] Q. Zhao, Z. Chang, X.D. Lei, X.M. Sun, *Ind. Eng. Chem. Res.*, 2011, 50, 10253–10258.

[39] Y.H. Chuang, Y.M. Zou, M.K. Wang, C.H. Liu, P.N. Chiang, *Ind. Eng. Chem. Res.*, 2008, **47**, 3813–3819.

[40] S.X. Xia, R.F. Nie, X.Y. Lu, L.N Wang, P. Chen, Z.Y. Hou, *J. Catal.*, 2012, **296**, 1–11.

[41] K.H. Goh, T.T. Lim, Z. Dong, *Water Res.*, 2008, **42**, 1343–1368.

[42] Z.J. Jia, Y. Wang and T. Qi, *RSC Adv.*, 2015, **5**, 62142-62148.

[43] L.P. Fang, W.T. Li, H.M. Chen, F. Xiao, L.Z. Huang, P.E. Holm, H.C.B. Hansen and D.S. Wang, *RSC Adv.*, 2015, **5**, 18866-18874.

[44] Z. Gu, J.J. Atherton, Z.P. Xu, *Chem.Comm.*, 2015, **51**, 3024-3036.

[45] X.H. Qiu, K. Sasaki, *Colloids Surf. A: Physicochem. Eng. Asp.*, 2015, **482**, 702–709

[46] W. Konicki, D. Sibera, E. Mijowska, Z. Lendzion-Bielun´, U. Narkiewicz, *J. Colloid Interface Sci.*, 2013, **398**, 152–160.

[47] Y. Song, C. Kong, J. Li, *Chinese. J. Chem. Phys.*, 2015, **28**, 84-90.

[48] J.T. Kloprogge, R.L. Frost, *J. Solid State Chem.*, 1999, **146**, 506-515.

[49] M.A. Butler, *J. Appl. Phys.*, 1977, **48**,1914-1920.

[50] P.G. Radaelli, *New J. phys.*, 2005, **7**, 53

[51] Y.S. Ho, *J. Hazard. Mater.*, 2006, **136**, 681–689.

[52] S.P. Govindwar, A.A. Telke, S.M. Joshi, S.U. Jadhav, D.P. Tamboli, *Biodegradation.*, 2010, **21**, 283–296.

[53] R.R. Shan, L.G. Yan, K.Yang, S.J. Yu, Y.F. Hao, H.Q. Yu, B. Du, *Chem. Eng. J.*, 2014, **252**, 38–46.

[54] X. Cheng, X.R. Huang, X.Z. Wang, B.Q. Zhao, A.Y. Chen, D.Z. Sun, *J. Hazard. Mater.*, 2009,**169**, 958–964.

[55] J.B. Zhou, S.L. Yang, J.G. Yu, Z. Shu, *J. Hazard. Mater.*, 2011,**192**, 1114–1121.

[56] X. Li, X.Chen, H. Niu, X. Han, T. Zhang, J.Y. Liu, H.M. Lin, F.Y. Qu, *J. Colloid Interface Sci.*, 2015, **452**, 89–97.

[57] C. Kong, J. Li, F.T. Liu, Y. Song and P. Song. *Desalin. Water. Treat.*, 2015.

[58] L.A. Pérez-Estrada, A. Agüera, M.D. Hernando, S. Malato, A.R. Fernández-Alba, *Chemosphere.*, 2008, **70**, 2068–2075.

[59] S.M. Wang, D.L. Li, C. Sun, S.G. Yang, Y. Guan, H. He, J. Mol. Catal. A Chem., 2014, **383–384,** 128–136.

[60] A. Elaziouti, N. Laouedj, A. Bekka, R.N. Vannier, *J. King Saud University-Science.*, 2015, **27**,

1 120–135.

Graphical Abstract

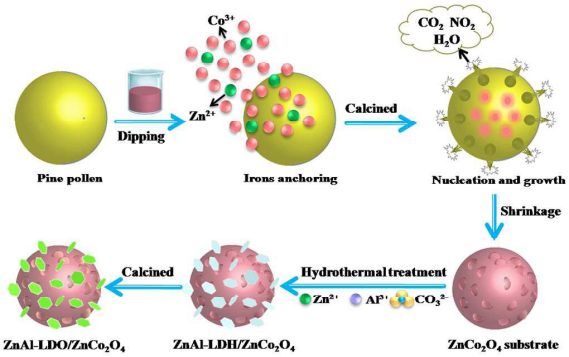

Schematic illustration of the synthesis of pollen-like ZnAl-LDH/$ZnCo_2O_4$ and its derived metal oxides